

## Phase diagram of optimally doped $\text{YBa}_2\text{Cu}_3\text{O}_{7-\delta}$ : Effect of oxygen stoichiometry

R. M. Langan, S. N. Gordeev,\* and P. A. J. de Groot

*Physics Department, Southampton University, Southampton, SO17 1BJ, United Kingdom*

A. G. M. Jansen

*Grenoble High Magnetic Field Laboratory, Max-Planck-Institut für Festkörperforschung  
and Centre National de la Recherche Scientifique, BP 166, 38042 Grenoble Cedex 09, France*

R. Gagnon and L. Taillefer

*Physics Department, McGill University, Montreal, Quebec, Canada H3A 2T8*

(Received 13 May 1998)

Influence of the oxygen stoichiometry on the phase diagram of clean  $\text{YBa}_2\text{Cu}_3\text{O}_{7-\delta}$  single crystals has been studied in the region of optimal doping ( $0.05 < \delta < 0.09$ ). Temperature and angular dependencies of magnetoresistance were analyzed for fields of up to 23 T. At low fields a sharp resistivity kink, which is a signature of the first order melting transition, was observed in all the samples studied. This kink, however, disappears when  $B$  exceeds the multicritical field  $B_{\text{mc}}$ . It was found that  $B_{\text{mc}}$  strongly increases with decreasing  $\delta$ . We have demonstrated that variations in the oxygen stoichiometry in the range of  $0.05 < \delta < 0.09$  do not have a significant effect on intrinsic parameters (such as anisotropy, coherence length, and penetration depth) but lead to a strong increase in entanglement of the vortex lines. We relate the dependence of  $B_{\text{mc}}$  on  $\delta$  with entanglement of the vortex lines, which is promoted by their interaction with oxygen vacancies.

[S0163-1829(98)01545-8]

### I. INTRODUCTION

Oxygen atoms play a very important role in the structure of  $\text{YBa}_2\text{Cu}_3\text{O}_{7-\delta}$ . It is known that small variations in oxygen stoichiometry can crucially change magnetic and transport properties of this compound. An increase in the oxygen deficiency  $\delta$  has three major effects. First of all, there are changes in the density of charge carriers which lead to a concomitant change in superconducting transition temperature  $T_c$  and magnetic penetration depth  $\lambda$ .<sup>1</sup> As was demonstrated by Breit *et al.*<sup>2</sup> in the region of low oxygen deficiency ( $\delta < 0.1$ ),  $T_c$  as a function of  $\delta$  shows a broad maximum at  $\delta \approx 0.05-0.08$ . Conventionally samples with oxygenations close to this peak in the  $T_c$  profile are referred to as being optimally doped.

Another important effect of the oxygen doping is to change in the anisotropy of effective masses  $\gamma = \epsilon^{-1} = (m_{ab}/m_c)^{-1/2} = (\xi_{ab}/\xi_c)$ , where  $\xi_{ab}$  and  $\xi_c$  are the coherence lengths parallel and perpendicular to the  $\text{Cu}_2\text{O}$  layers, respectively. As oxygen atoms are removed  $\xi_c$  decreases, whereas  $\xi_{ab}$  remains approximately constant thereby driving the system more two dimensional.<sup>3</sup>

The third effect is that as the oxygen atoms are removed the number of point defects (oxygen vacancies in the crystalline lattice) increase. Because of the short coherence length in  $\text{YBa}_2\text{Cu}_3\text{O}_{7-\delta}$  departure from stoichiometry at even a single atomic site is sufficient to locally depress the superconducting order parameter. Simple estimations<sup>4</sup> show that single oxygen vacancies cannot be effective pinning centres at temperatures close to  $T_c$ . However, in clean  $\text{YBa}_2\text{Cu}_3\text{O}_{7-\delta}$  single crystals, dynamic interactions of the moving vortices with single oxygen vacancies and clusters of vacancies are expected to promote vortex entanglement and

increase the viscosity of the vortex liquid.<sup>5</sup> This would explain the deviation from the Bardeen-Stephen flux flow model observed just above the vortex lattice melting temperature.<sup>6</sup>

The interactions of the vortices with oxygen vacancies are, however, completely obscured in  $\text{YBa}_2\text{Cu}_3\text{O}_{7-\delta}$  samples which have been strongly contaminated by impurities or irradiated with ion beams. In such cases pinning by impurities or columnar defects becomes a predominant effect.<sup>5</sup> In order to observe the interaction of vortices with oxygen vacancies it is necessary to have sufficiently clean samples, for which these defects are the main pinning centers. This requirement is especially important for studies of optimally doped or overdoped samples for which the density of oxygen vacancies is low. In most of the earlier studies the samples were apparently not clean enough. For such samples the effects of oxygen stoichiometry on transport and magnetic properties were found to be very weak for  $\delta < 0.1$ .<sup>1</sup> However, recent magnetization studies on cleaner samples<sup>7-9</sup> have demonstrated a dramatic effect of oxygenation on the magnitude of shielding currents as well as their field and temperature dependencies.

An  $\text{YBa}_2\text{Cu}_3\text{O}_{7-\delta}$  single crystal can be identified as being clean if a first order phase transition from the vortex solid to the vortex liquid state is observed. It has been demonstrated<sup>10</sup> that in such samples this transition manifests itself as a very sharp ‘‘kink’’ in resistivity as function of temperature or field. At high fields, above the so called multicritical field  $B_{\text{mc}}$ , the ‘‘kink’’ in the  $\rho(T)$  curves is smoothed out.<sup>11</sup> Very recent specific heat measurements have revealed that for  $B > B_{\text{mc}}$  the liquid-to-solid transition becomes second order.<sup>12</sup> It was also observed that decreases in  $\delta$  drive the multicritical point to higher fields. However,

TABLE I. Annealing temperature  $T_{\text{anneal}}$ , oxygen concentration  $7-\delta$ , critical temperature  $T_c$ , transition width  $\Delta T_c$ , and normal state resistivity  $\rho_n$  for the samples studied.

Sample	$T_{\text{anneal}}(^{\circ}\text{C})$	$7-\delta$	$l \times w \times t(\text{mm}^3)$	$T_c$ (K)	$\Delta T_c$ (K)	$\rho_n(\mu\Omega \text{ cm})$
Y1	525	6.91	$1.23 \times 0.89 \times 0.14$	93.3	0.3	56
Y2a	500	6.93	$1.14 \times 0.73 \times 0.07$	93.6	0.3	73
Y2b	475	6.95	$0.64 \times 0.75 \times 0.07$	93.2	0.6	63

specific heat measurements do not allow the vortex dynamics to be studied, thus mechanisms, which could be responsible for such transformations of the melting line, were not analyzed.

In this paper we study the effect of oxygen stoichiometry upon the properties of clean  $\text{YBa}_2\text{Cu}_3\text{O}_{7-\delta}$  single crystals in the region of optimal doping ( $0.05 < \delta < 0.09$ ). By choosing appropriate oxygen annealing conditions we were able to prepare three samples with characteristically different oxygenations, such that these samples were slightly underdoped, optimally doped, and slightly overdoped, respectively. From studies of resistivity versus temperature, versus field and versus angle between this field and the  $c$  axis, we have concluded that parameters such as anisotropy, upper critical field, the field dependent melting temperature vary only slightly between the three samples. In contrast, we observed large (greater than a factor of 2) decreases in  $B_{\text{mc}}$  as  $\delta$  increases. We have subsequently demonstrated that this effect can be explained in terms of an increase in the entanglement of vortices as promoted by their interaction with oxygen vacancies.

## II. EXPERIMENTAL SETUP

The results presented in this paper were obtained from two twinned  $\text{YBa}_2\text{Cu}_3\text{O}_{7-\delta}$  single crystals, grown using a self-flux method in an yttria stabilised zirconia crucible.<sup>13</sup> In order to vary the oxygen concentration of the samples, we annealed them in flowing  $\text{O}_2$  at different temperatures. The values for the oxygen deficiency  $\delta$  were then deduced from the calibration curves of Ref. 14. Initially the crystals were annealed for 7 days at a temperature of 500  $^{\circ}\text{C}$  which should lead to an optimal oxygen concentration  $7-\delta=6.93$  ( $\delta=0.07$ ). The samples with this oxygen concentration were found to have the highest critical temperatures ( $T_c=93.6$  K) of the  $\text{YBa}_2\text{Cu}_3\text{O}_{7-\delta}$  samples which we have studied. One of these crystals, (sample Y1) was then annealed for a further seven days at a temperature of 525  $^{\circ}\text{C}$  so that the oxygen concentration would be changed to  $7-\delta=6.91$  ( $\delta=0.09$ ). The other crystal, Y2, after initial oxygenation at 500  $^{\circ}\text{C}$ , was cut into two sections (samples Y2a and Y2b). One of these pieces was reoxygenated at a temperature of 475  $^{\circ}\text{C}$  (sample Y2b) so that it would have oxygen concentration  $7-\delta=6.95$ .<sup>14</sup> The zero field transition temperature  $T_c$  [determined from the condition  $\rho(T_c)=0.5\rho(95 \text{ K})$ ] and its width  $\Delta T_c$  (10–90 %) are presented in Table I for each of these samples. It can be seen that the critical temperature  $T_c$  is slightly lower for crystals Y1 and Y2b than for crystal Y2a. We refer to the sample with maximum  $T_c$  (sample Y2a) as being optimally doped and the samples Y1 and Y2b as under and overdoped, respectively. Table I also lists the dimensions of the three crystals.

Current contacts were attached to the sides of the samples to provide a uniform current flow along the  $ab$  plane. Transport measurements were performed using a standard lock-in techniques with square wave modulated currents  $f_m=88$  Hz. The magnitudes of currents were 0.6, 1.0, and 0.5 mA for samples Y1, Y2a, and Y2b, respectively. Most of the data were taken using a 14 T cryomagnet but some of the measurements, over an extended field range of up to 23 T, were carried at the Grenoble High Magnetic Field Laboratory (GHMFL). For some of our measurements the angle ( $\theta$ ) between the  $c$  axis and the applied field was varied but in all cases the field remained perpendicular to the applied current.

## III. RESULTS

We have performed extensive transport measurements on all three samples. For brevity we concentrate on a comparison of the results for the two crystals Y1 ( $\delta=0.09$ ) and Y2b ( $\delta=0.05$ ) which represent the extremes in the range of oxygen concentration considered by this study. In all cases, where it would be expected to do so, the optimally doped sample Y2a ( $\delta=0.07$ ) demonstrated behavior which was intermediate between these two extremes.

Figures 1(a) and 1(b) present the normalized resistivity versus temperature dependencies  $[\rho(T)/\rho_n]$  of crystals Y1 and Y2 for various different fields in the range  $B=0-14$  T. Here we take the normal state resistivity  $\rho_n$  to the value at  $T=100$  K. In all cases the fields were applied at an angle of  $\theta=15^{\circ}$  to the crystalline  $c$  axis. As demonstrated in our previous paper,<sup>15</sup> in this geometry pinning by twin boundaries is suppressed and a twinned crystal behaves as though it was detwinned.

For applied magnetic fields  $B \leq 5$  T, the resistivity curves for crystal Y1 [Fig. 1(a)] exhibit a kink at  $\rho(T)/\rho_n \approx 0.08$  representing the first order melting/freezing transition at  $T_m$  between vortex solid and liquid states.<sup>10,12,16</sup> For larger fields, the kink is suppressed such that instead of dropping off sharply at  $T_m$  the curves fall off gradually towards zero. Following Safar *et al.*,<sup>11</sup> we have associated this field-induced broadening of the resistivity transition with the so called multicritical point, this being the point at which the first order melting transition is driven second order.

For crystal Y2b [Fig. 1(b)] the melting kink is visible at  $\rho(T)/\rho_n \approx 0.12$  for fields of up to  $B=13$  T. Only above this much larger field do the  $\rho(T)$  curves begin to broaden. Similar measurements for crystal Y2a show that a critical field, above which the kink is suppressed, of  $B=11$  T. The inset to Fig. 1(a) presents the evolution of the width of the resistive transition  $\Delta T$  (defined as the temperature difference between the arbitrary resistivity criteria,  $0.05\rho_n$  and  $0.02\rho_n$ ) for each of the crystals as a function of effective field,  $B_{\text{eff}}$ . The increase in the oxygenation shifts the  $\Delta T(B_{\text{eff}})$  curve to higher

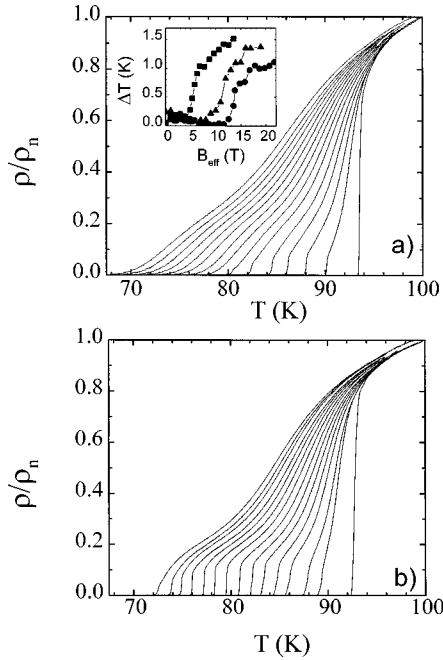


FIG. 1. Temperature dependence of normalized resistivity curves for (a) an underdoped sample Y1 ( $\delta=0.09$ ) and (b) an overdoped sample Y2b ( $\delta=0.05$ ). Magnetic fields  $B=0-14$  T (step 1 T) were applied at an angle of  $15^\circ$  to the  $c$  axis. Inset: the width of the melting transition,  $\Delta T$ , for the samples Y1, Y2a, and Y2b (from left to right) as a function of effective field  $B_{\text{eff}}=B \cos 15^\circ$ .

fields. For  $\text{YBa}_2\text{Cu}_3\text{O}_{7-\delta}$  single crystals it is known that the effective field can be calculated from the expression  $B_{\text{eff}}=B\varepsilon_\theta$ .<sup>17</sup> Here  $\varepsilon_\theta$  is the angular dependent anisotropy factor given by  $\varepsilon_\theta=(\cos^2\theta+\varepsilon^2\sin^2\theta)^{1/2}$ . For a relatively small angle of inclination,  $\theta=15^\circ$ , this effective field approximates to  $B_{\text{eff}}=B \cos 15^\circ$ . We define the effective field at which the width of the melting transition increases sharply as the multicritical field  $B_{\text{mc}}$ . As shown in the Table II,  $B_{\text{mc}}$  increases with decreasing oxygen deficiency, from 5.5 T for the underdoped sample Y1 to 13 T for the overdoped sample Y2b.

Figure 2 is a comparison of the angular dependences of the resistivity for crystals Y1 and Y2b taken at a number of temperatures in an applied field of  $B=5$  T (which lies below the multicritical field for both samples). Both crystals exhibit a sharp minimum in the resistivity when the magnetic field is applied parallel to the  $c$  axis ( $\theta=0^\circ$ ), a feature which has been associated with pinning by twin boundaries.<sup>18</sup> Figure 2 demonstrates that the angular range over which there is a suppression in the resistivity, is larger for the crystal with the lowest oxygen concentration (Y1). For this sample the dip extends out to  $\theta_{\text{TB}}=13^\circ$ , whereas for crystal Y2b it is confined to  $\theta_{\text{TB}}=6^\circ$ . The important point to draw from these

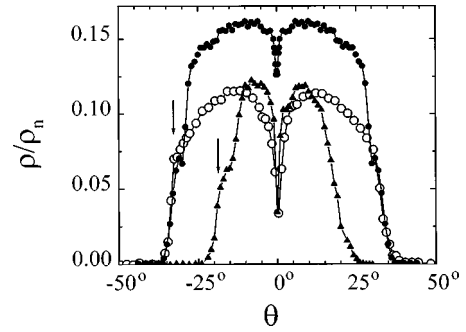


FIG. 2. Normalized resistivity for the samples Y1 (open symbols) and Y2b (closed symbols) as a function of angle  $\theta$  between the applied field (5 T) and the  $c$  axis. Temperatures are 83.8 K (open circles), 84.18 K (closed circles), and 83.36 K (triangles). Arrows show the melting angles  $\theta_m$ .

$\rho(\theta)$  dependencies is that, the  $\rho(T)$  curves of Fig. 1 (and any further measurements taken at an angle of  $\theta \geq 15^\circ$ ) should not be affected by twin boundary pinning.

Figure 2 also demonstrates that, for both overdoped and underdoped samples, as angle is increased above  $\theta_{\text{TB}}$  at first the resistivity decreases smoothly until at one point it drops abruptly. The angle at which this drop occurs has been called the *melting angle*  $\theta_m$  (Ref. 15) (indicated by the arrows in Fig. 2) and decreases with decreasing temperature. This ‘‘kink’’ on the  $\rho(\theta)$  dependence can be associated with the ‘‘kink’’ arising in the  $\rho(B)$  curve where the melting line is crossed. The difference is that in the latter case the magnitude of the applied field at constant  $\theta$  is changed but in the former case the effective field is changed by tilting the sample. In Fig. 2 the samples are in the vortex liquid state for  $\theta < \theta_m$ . Upon increasing the angle  $\theta$ , the effective field  $B_{\text{eff}}=B\varepsilon_\theta$  decreases and at  $\theta=\theta_m$  (for which  $B_{\text{eff}}=B_m$ ), the vortex liquid freezes giving a sharp drop in resistivity.

If the vortex dynamics were determined entirely by the effective field  $B_{\text{eff}}=B\varepsilon_\theta$ , then tilting the sample at a constant applied field would have exactly the same effect as a reduction in the magnitude of applied field at a constant angle  $\theta$ . However we have found that this ‘‘effective field’’ approximation does not work for angles close to  $90^\circ$ . Figure 3(a) presents  $\rho(T)$  curves for crystal Y1 when a field of  $B=5$  T is applied at a number of angles in the range  $\theta=0^\circ-90^\circ$ . Figure 3(b) presents similar data for crystal Y2b for the same magnitude of applied field  $B$ . In both figures the effective field ( $B_{\text{eff}}$ ) is less than the multicritical field for all of the curves, with the exception of those for  $\theta=0^\circ$  for which there is an additional influence due to twin boundary pinning.

The inset to Fig. 3(a) is a comparison, for underdoped crystal Y1, of the  $\rho(T)$  curve for  $\theta=15^\circ$  and  $B=1$  T with

TABLE II. Oxygen concentration  $7-\delta$ , multicritical field  $B_{\text{mc}}$ , anisotropy parameter  $\varepsilon$ , slope of the upper critical field line  $\beta=dB_{c2}/dT$ , in-plane coherence length  $\xi_{ab}$ , parameter  $B_0$  of the fit of the melting line  $B_m=B_0(1-T/T_c)^\alpha$ , and misalignment angle  $\zeta_{\text{mis}}$  for  $\text{YBa}_2\text{Cu}_3\text{O}_{7-\delta}$  single crystals.

Sample	$7-\delta$	$B_{\text{mc}}$ (T)	$\varepsilon$	$\beta$ (T/K)	$\xi_{ab}$ ( $\text{\AA}$ )	$B_0$ (T)	$\zeta_{\text{mis}}$ ( $^\circ$ )
Y1	6.91	5.5	0.130	2.04	13.2	103	10
Y2a	6.93	11	0.134	2.10	12.9	115	8
Y2b	6.95	13	0.148	2.27	12.5	118	2

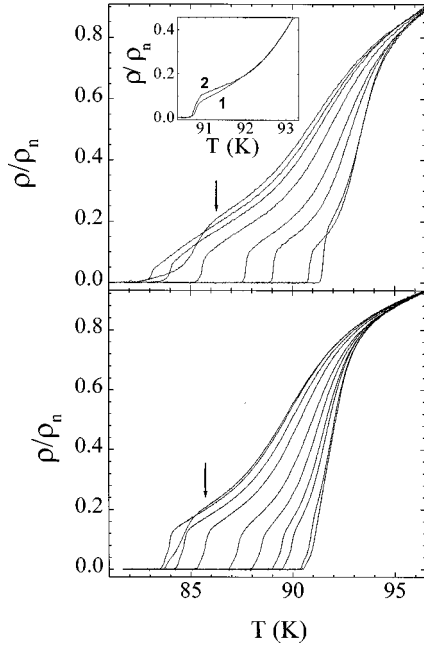


FIG. 3. Normalized resistivity as a function of temperature for samples Y1 (upper panel) and Y2b (lower panel). The measurements were performed in a field of  $B=5$  T, for different angles. From left to right:  $\theta=0^\circ, 15^\circ, 30^\circ, 45^\circ, 62.5^\circ, 72.5^\circ, 85^\circ, 90^\circ$  (upper panel); and  $\theta=0^\circ, 15^\circ, 30^\circ, 45^\circ, 60^\circ, 70^\circ, 80^\circ, 82^\circ, 87^\circ, 90^\circ$  (lower panel). Arrows show the onset of twin boundary pinning for  $\theta=0^\circ$ . The inset compares two  $\rho(T)$  curves for sample Y1, obtained with  $\theta=15^\circ$  at  $B=1$  T (curve 1) and  $\theta=85^\circ$  at  $B=5$  T (curve 2).

that for  $\theta=80^\circ$  and  $B=5$  T. The sharp resistivity drop occurs at the same temperature  $T_m=89$  K in both cases, which means that the effective field is the same. In spite of this, the curve measured at  $\theta=80^\circ$  demonstrates an excess resistivity above the melting kink. The excess resistivity strongly increases as  $\theta=90^\circ$  is approached. It can be seen from the main panel of Fig. 3(a), that for  $\theta=90^\circ$  the excess resistivity is so high that the curve intersects the  $\rho(T)$  curve for the smaller angle of  $\theta=85^\circ$ . For the overdoped sample Y2b the excess resistance at  $\theta=90^\circ$  is much smaller and the curves for different  $\theta$  did not intersect each other at any point [see Fig. 3(b)].

#### IV. DISCUSSION

##### The melting line $B_m(T)$

To construct melting lines for our samples we have used  $\rho(T)$  data similar to that presented in Fig. 1, extracting melting temperatures  $T_m$  using an arbitrary resistivity criterion  $\rho(T)/\rho_n=0.05$ . For fields below  $B_{mc}$  the melting kink is very sharp and the  $T_m$  values obtained in this way were practically independent of the particular criterion. However, this method cannot be used above  $B_{mc}$  where the resistivity transition broadens. Safar *et al.*<sup>11</sup> have demonstrated that for  $B > B_{mc}$  the resistivity tail can be described by the ‘‘vortex glass’’ theory<sup>19</sup> and the  $\rho(T)$  dependence is well fitted by the relation  $\rho(T) \sim (T - T_g)^s$ , with  $s=6$ . Following Ref. 11, we have plotted  $\rho(T)^{1/6}$  as a function of temperature and ob-

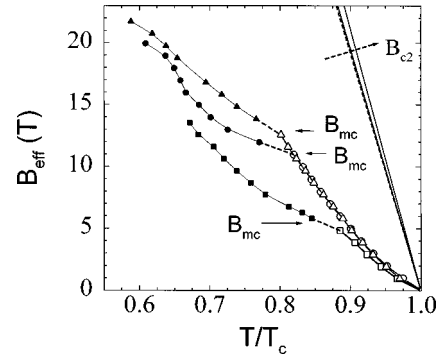


FIG. 4. Phase diagram for  $\text{YBa}_2\text{Cu}_3\text{O}_{7-\delta}$  showing the effect of varying oxygen content. Open symbols represent the melting lines  $B(T_m)$  and closed symbols show the ‘‘vortex glass’’ lines  $B(T_g)$  for samples: Y1 (squares), Y2a (circles), and Y2b (triangles). The multicritical points  $B_{mc}$  have been indicated with arrows. The upper critical field  $B_{c2}(T)$  lines are also shown, the arrow indicates the direction of increasing oxygen concentration.

tained the glass temperature  $T_g$  for a particular field by extrapolating of the linear section of this curve to  $\rho=0$ . The glass temperature  $T_g$  has then been plotted on the phase diagram for its corresponding effective field  $B_{\text{eff}}$ . From Fig. 4 one can see that, for a particular crystal, the glass/liquid phase line joins the melting line at the multicritical point. Also, as the oxygen concentration is increased the glass scaling line is driven to higher fields.

Analysis of the data below  $B_{mc}$  has shown that while the  $B_m(T/T_c)$  curves for the optimally doped and overdoped samples coincide closely, the melting line for the underdoped sample is different. We find that for all samples the melting lines below  $B_{mc}$  fit well to the equation  $B_m = B_0(1 - T/T_c)^\alpha$  with the same power index  $\alpha=1.39$ . However, the prefactor  $B_0$  is found to be different (see Table II).

Theory<sup>17</sup> predicts the following formula for the melting line:

$$B_m = \frac{\Phi_0^5 c_L^4 \epsilon^2}{16\pi^4 (k_B T)^2 \lambda_{ab}^4 \epsilon_\theta}, \quad (1)$$

where  $\Phi_0$  is the flux quantum,  $c_L$  is the Lindemann number,  $\lambda_{ab}$  is the London penetration depth in the  $ab$  plane, and  $\epsilon_\theta$  is the angular dependent anisotropy ratio defined according to  $\epsilon_\theta = (\cos^2\theta + \epsilon^2 \sin^2\theta)^{1/2}$ . It has been demonstrated experimentally<sup>15,20</sup> that the angular dependence of the melting line for clean optimally doped  $\text{YBa}_2\text{Cu}_3\text{O}_{7-\delta}$  single crystals closely follows this relation. As was shown above, small variations in  $\delta$  do not change the temperature dependence of the melting line. The observed change in the prefactor  $B_0$  is apparently related to changes in the anisotropy and density of charge carriers  $n_{\text{ch}}$  (and correspondingly in  $\lambda_{ab} \propto n_{\text{ch}}^{-0.5}$ ).

As can be seen from Eq. (1), the anisotropy of samples can be estimated from a comparison of the melting lines for  $\theta=0^\circ$  and  $\theta=90^\circ$ . The anisotropy factor  $\epsilon$  is simply the ratio of the melting fields  $B_m(90^\circ)/B_m(0^\circ)$  obtained at the same temperature. As shown in Table II  $\text{YBa}_2\text{Cu}_3\text{O}_{7-\delta}$  single crystals become less anisotropic with increasing oxygenation. This is in agreement with recent specific heat measurements of anisotropy for highly oxygenated  $\text{YBa}_2\text{Cu}_3\text{O}_{7-\delta}$ .<sup>12</sup> A similar continuous change of anisotropy

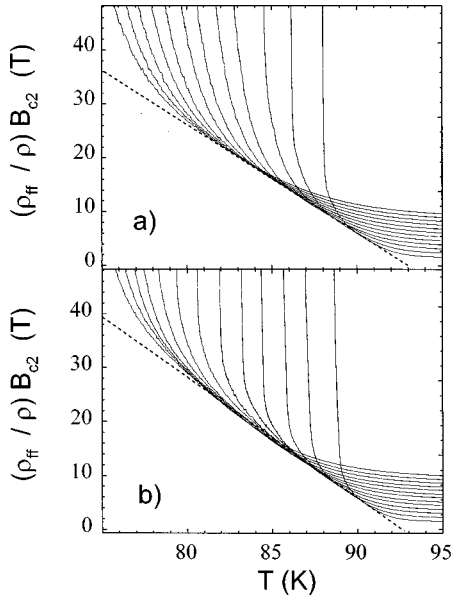


FIG. 5. Variation of the function  $(\rho_{ff}/\rho)B_{c2} = \varepsilon_{\theta} B \rho_n / \eta \rho$  with temperature for samples Y1 (a) and Y2b (b). The data demonstrate the scaling behavior of the  $\rho(T)$  curves presented in Figs. 1(a) and 1(b), respectively. The linear dependence yields the upper critical field lines  $B_{c2}(T)$ .

over a wide range of oxygen doping was observed for  $\text{HgBa}_2\text{CuO}_{4+\delta}$ .<sup>21</sup> The decrease in the anisotropy gives contribution to the observed change in the melting line. Unfortunately we cannot elucidate the role of another factor ( $\lambda_{ab}$ ) because the accuracy of our measurements of the anisotropy ( $\sim 3\%$ ) is not high enough to analyze quantitatively the observed small variations in the melting line.

#### Flux-flow scaling

In our recent paper<sup>15</sup> we showed that for small angles ( $\theta \leq 60^\circ$ ) substantial sections of the  $\rho(T)$  curves below  $T_c$  exhibit ideal flux flow scaling. According to Ivlev and Kopnin,<sup>22</sup> in the field range  $\mu_0 H_{c1} \ll B \ll B_{c2}$ , the ratio of flux-flow resistivity to normal state resistivity can be written as

$$\frac{\rho_{ff}(\theta, T)}{\rho_n(T)} = \frac{\varepsilon_{\theta} B}{\eta B_{c2}(0, T)}, \quad (2)$$

where  $\eta = 1.45$  is a constant.

We used this relation to extract values of  $B_{c2}$  for our samples. Figure 5 is a comparison of the temperature dependencies of the function  $\varepsilon_{\theta} B \rho_n(T) / \eta \rho(T) = (\rho_{ff}/\rho) B_{c2}$ , where the  $\rho(T)$  values have been taken from Fig. 1 and the  $\rho_n(T)$  dependence is a linear extrapolation of the resistivity from the high temperature region. On comparison of this function with Eq. (2) it becomes clear that it should yield the value of the upper critical field in the temperature intervals for which the vortex dynamics is determined by free flux-flow. Figure 5 shows that, for a particular crystal, if the  $(\rho_{ff}/\rho) B_{c2}$  curves for all fields are plotted together on the same graph then a linear dependence emerges. This dependence indicates the variation of the upper critical field with temperature and can be represented by  $B_{c2} = \beta(T_c - T)$ . The

proportionality factor  $\beta$  shows weak dependence on the oxygen deficiency increasing only by about 10% as  $\delta$  changes from 0.09 to 0.04. This means that the coherence length  $\xi_{ab}$ , which is related to the upper critical field [ $B_{c2} = \Phi_0 / (2\pi\xi_{ab}^2)$ ], is practically the same for all three samples (see Table II). The upper critical field lines,  $B_{c2}(T)$ , have been plotted on the phase diagram (Fig. 4) and the dashed arrow indicates the direction of increasing oxygen concentration.

#### Role of the vortex entanglement

Fendrich *et al.*<sup>4</sup> have demonstrated that deviation from the flux flow resistivity in the vicinity of  $T_m$  can be related to point disorder. They have found that when point defects are introduced into a crystal (by irradiation with 1 MeV electrons), both the flux-flow behavior and the melting transition were suppressed. Pinning by point disorder at temperatures  $T > T_m$  is not effective since the corresponding pinning potential is small compared to  $k_B T$ .<sup>4</sup> However, Nelson<sup>23</sup> proposed that thermal disorder leads to vortex entanglement in the liquid state. The dynamic interaction of moving vortices with the point defects create modulations in the vortex velocity and increases the viscosity of the vortex liquid thus leading to a decrease in the resistivity.<sup>6,15</sup>

It is surprising, but when the magnetic field is applied at small angle to the  $ab$  plane entanglement increases rather than decreases the resistivity. This can be seen in Fig. 3(a) as the crossover of the  $\rho(T)$  curves for  $\theta = 90^\circ$  and  $\theta = 85^\circ$ . Due to the anisotropic structure of  $\text{YBa}_2\text{Cu}_3\text{O}_{7-\delta}$ , the Lorentz force acting on a small element  $dl$  of the vortex line will depend on the inclination angle ( $\zeta$ ) of this line relative to the crystalline  $ab$  plane. The force on this unit element is thus given by  $df = JB(\sin^2\zeta + \varepsilon^2\cos^2\zeta)^{1/2} dl / \varepsilon$ . This force is minimum when the vortex line is parallel to the  $ab$  plane ( $\zeta = 0$ ). Thus, when the field direction is close to the  $ab$  plane, the bending of the vortex lines anomalously increases the effective Lorentz force and leads to an increase in the resistivity which we term the excess resistivity. This effect is the most pronounced when the field is applied along the  $ab$  plane and quickly falls off as the angle between the field direction and the  $ab$  plane increases.<sup>24</sup> As can be seen from Fig. 2(a), the excess resistivity is much higher for  $B \parallel ab$  ( $\theta = 90^\circ$ ) than for  $\theta = 85^\circ$  resulting in an intersection of the  $\rho(T)$  curves for these two different angles.

In Ref. 15 it was suggested that the strength of the vortex entanglement could be characterized by an ‘‘effective misalignment’’ angle,  $\zeta_{ms}$ . This angle represents the inclination, between the field and the  $ab$  plane, at which disentangled vortex liquid gives the same resistivity as an entangled vortex liquid for  $\theta = 90^\circ$ . The misalignment angle can be estimated from a comparison of experimental  $\rho(\theta = 90^\circ)$  values with  $\rho_{ff}$  for a disentangled vortex liquid in the vicinity of  $\theta = 90^\circ$ . Figure 6 shows a  $\rho(T, \theta = 90^\circ)$  curve for the sample Y1 at  $B = 5$  T. It is compared with flux-flow resistivity for disentangled vortex liquid,  $\rho_{ff}(T, \theta = 90^\circ)$ , calculated from Eq. (2). As was discussed above, entanglement increases flux flow resistivity for  $\theta$  close to  $90^\circ$  thus the experimental  $\rho(T, \theta = 90^\circ)$  curve lies above the  $\rho_{ff}(T, \theta = 90^\circ)$  dependence. For temperatures just above  $T_m$ , it coincides with the flux-flow resistivity of disentangled liquid for another angle,

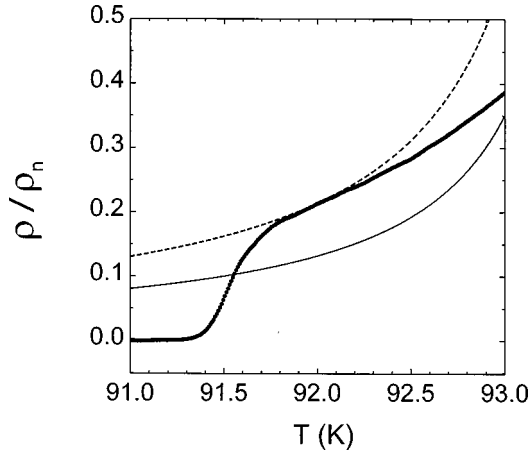


FIG. 6. Comparison of the  $\rho(T, \theta=90^\circ)$  curve for sample Y1 at  $B=5$  T (symbols) with the  $\rho_{ff}(T, \theta=90^\circ)$  and  $\rho_{ff}(T, \theta=80^\circ)$  dependences for disentangled liquid (thin line and dashed line, respectively).

$\rho_{ff}(\theta=90^\circ - \zeta_{ms})$  with  $\zeta_{ms}=10^\circ$  (dashed line in Fig. 6). This means that the entanglement-induced misalignment of the vortex lines can be estimated as  $10^\circ$ . Similar analysis gives the  $\zeta_{ms}$  values of  $8^\circ$  and  $2^\circ$  for the samples Y2a and Y2b, respectively. Thus the strength of the vortex entanglement increases with increasing oxygen deficiency  $\delta$ .

Entanglement has an important impact to the interaction of the vortex lines with twin boundaries. In the case of a disentangled liquid, for a magnetic field oriented at an arbitrary angle relative to the twin planes, the configuration of a vortex lines is usually considered to be determined by two competing energy contributions<sup>5</sup>: (i) the gain in energy due to pinning by twin planes; (ii) the cost of elastic energy in bending the vortex lines away from the direction of internal magnetic field. As a result of this competition the vortices have a kinked structure at low tilting angles  $\theta$ . When the tilting angle increases above some critical value  $\theta_{tr}$  (the trapping angle) kink formation becomes energetically unfavorable and beyond this point twin boundaries have no further influence on the vortex motion. For  $\theta > \theta_{tr}$  the angular dependence of resistivity is practically the same as for a detwinned sample.

If the vortices are entangled, different sections of vortex lines have different angles with respect to the twin boundary planes. In this case, the vortices cease to interact with the twin boundary at an angle  $\theta_{TB} = \theta_{tr} + \zeta_{ms}$  where  $\theta_{TB}$  is the critical angle for twin boundary pinning in the absence of vortex entanglement and  $\zeta_{ms}$  is the effective misalignment angle arising due to entanglement. This effect could explain why, in Fig. 2, the effect of twin boundary pinning extends out to larger angles for the sample with higher oxygen deficiency. The difference between the measured angles  $\theta_{TB}$  for samples Y1 and Y2b is  $7^\circ$ , which corresponds closely to the difference between the calculated  $\zeta_{ms}$  values for these samples.

#### Multicritical point

The results presented in Fig. 4 show that the multicritical point which separates two different regimes of the vortex solid melting (first and second order phase transitions) is

very sensitive to the oxygen deficiency. A similar effect was observed by Khaykovich *et al.*<sup>25</sup> in  $\text{Bi}_2\text{Sr}_2\text{CaCu}_2\text{O}_{8+\delta}$  single crystals. On annealing a  $\text{Bi}_2\text{Sr}_2\text{CaCu}_2\text{O}_{8+\delta}$  sample in oxygen, the endpoint of the first order melting transition was observed to shift to higher fields. However, this effect was accompanied by a substantial increase in the values of the melting field, which would indicate that the intrinsic parameters of the material ( $\epsilon$ ,  $\lambda$ ) were also changed. Therefore, the effect of the oxygen annealing was not only to decrease the point defect density, but also to decrease the elementary interaction force between the vortices and the defects. It seems, that the latter effect was much more pronounced, since the temperature corresponding to the multicritical point,  $T_{mc}$  was increased rather than decreased during the annealing process. Khaykovich *et al.*<sup>25</sup> have demonstrated that when the density of point defect in  $\text{Bi}_2\text{Sr}_2\text{CaCu}_2\text{O}_{8+\delta}$  is changed without changing the intrinsic parameters (they achieved this through electron irradiation of the sample) then  $T_{mc}$  decreases but the melting line does not change.

In our experiments we have observed that oxygen annealing of optimally doped  $\text{YBa}_2\text{Cu}_3\text{O}_{7-\delta}$  crystals has a minor effect on intrinsic parameters such as  $\epsilon$ ,  $\lambda$ ,  $\xi$ . The only parameter that was changed substantially was the density of oxygen defects. As in the case of irradiated  $\text{Bi}_2\text{Sr}_2\text{CaCu}_2\text{O}_{8+\delta}$  the increase of point defects resulted in a strong shift of the multicritical point to higher fields and lower temperatures without substantial changes in the position of the melting line.

The results obtained provide an explanation for the apparent discrepancies, as observed in magnetic measurements, between the behavior of contaminated and clean  $\text{YBa}_2\text{Cu}_3\text{O}_{7-\delta}$  for oxygenations in the range  $(7-\delta) > 6.9$ . While for contaminated samples no significant effect of oxygen annealing was observed,<sup>1</sup> in the case of pure samples magnetic measurements showed very strong changes with oxygenation of both the magnitude and the field dependence of shielding currents  $J_{sh}$ .<sup>7-9</sup> In contaminated samples the main pinning centers are impurities therefore oxygen annealing does not significantly alter the density of pinning centers. Our results indicate that the intrinsic parameters are only weakly dependent on  $\delta$ , therefore the variation in the elementary force of interaction between the vortices and these centers is also small. In the case of clean  $\text{YBa}_2\text{Cu}_3\text{O}_{7-\delta}$  the main pinning centers are oxygen vacancies (and clusters of vacancies). As  $\delta$  decreases, the density of pinning centers drops reducing  $J_{sh}$ . At the same time, as was demonstrated above, the vortex glass melting line moves to higher fields pushing the irreversibility line upwards and changing the  $J_{sh}(B)$  dependence.

To date, it is unresolved as to why the first order melting transition should terminate at higher fields: this is a subject of intense theoretical investigations. According to one point of view,<sup>11</sup> the first order melting transition is robust in the presence of a certain amount of disorder. When this level is exceeded, the transition becomes second order. It is argued that, in the presence of a constant amount of quenched disorder, a similar effect can be induced by increasing the applied magnetic field. The effect of the magnetic field is to shift the melting transition to lower temperatures where the interaction of vortices with pinning centers is stronger. This

will lead to an increase in the importance of disorder and to suppression of the first order melting transition.<sup>26</sup>

According to the alternative point of view,<sup>26,27</sup> the shift in the multicritical point is due to an increase in the entanglement of the vortex liquid with an associated increase in its viscosity. Entanglement would prevent crystallization of the vortex liquid instead producing a nonequilibrium but continuous “polymer-glass” transition.<sup>26</sup> It is expected that weak point disorder should promote vortex entanglement. Thus in the framework of this entanglement interpretation, increases in oxygen deficiency should push the multicritical point to lower fields and higher temperatures.<sup>26,27</sup>

In fact, since the predictions of these two models regarding the response of the multicritical point to changes in  $\delta$  are so similar that it is impossible to distinguish between them in this respect. However, what our studies have unequivocally demonstrated is that the influence of vortex entanglement does increase significantly with both magnetic field and oxygen deficiency. This observation provides experimental support for the entanglement related explanation for the suppression of the first order melting transition.

In conclusion, we have performed studies of magnetoresistivity in clean  $\text{YBa}_2\text{Cu}_3\text{O}_{7-\delta}$  single crystals for a range of different oxygenations  $\delta$  ( $0.05 < \delta < 0.09$ ) in the vicinity of optimal doping. The relative “cleanness” of the samples was confirmed by observation of the sharp resistivity kinks at  $T_m$  which are a signature of a first order melting transition.

The melting line was observed to terminate at high fields and the multicritical point marking the end of the melting line was found to be strongly dependent on the oxygen deficiency. We have demonstrated that for all the samples which we studied over the range of fields 0–23 T there existed a temperature region where the dissipation was due to free flux flow. In the vicinity of the melting/freezing transition the measured resistivity deviated from the flux-flow resistivity. We have found that this deviation is strongly dependent on (i) the density of oxygen defects, (ii) the magnitude of the applied field, and (iii) the tilting angle between the field and the *ab* plane. We have demonstrated that all of these dependencies can be attributed to entanglement of the vortex lines. The strength of entanglement increases with increasing magnetic field or oxygen deficiency leading to a suppression of the first order melting transition at the multicritical point.

#### ACKNOWLEDGMENTS

This project was funded by the EPSRC (UK) and has also been supported by the “Training and Mobility of Researchers” Programme of the European Community under Contract No. ERBFMGECT950077. R.G. and L.T. acknowledge funding from NSERC (Canada), FCAR of Quebec and CIAR (Canada). L.T. acknowledges the support of the Sloan Foundation.

\*On leave from the Moscow Institute of Radioengineering, Electronics and Automation, 117454 Moscow, Russia. Author to whom all correspondence should be addressed.

<sup>1</sup>J. G. Ossandon, J. R. Thompson, D. K. Christen, B. C. Sales, H. R. Kerchner, J. O. Thompson, Y. R. Sun, K. W. Lay, and J. E. Tkaczyk, *Phys. Rev. B* **45**, 12 534 (1992); L. Tallon, C. Bernard, H. Shaked, R. L. Hitterman, and J. D. Jorgensen, *ibid.* **51**, 12 911 (1995).

<sup>2</sup>V. Breit, P. Schweiss, R. Hauff, H. Wühl, H. Claus, H. Rietschel, A. Erb, and G. Müller-Vogt, *Phys. Rev. B* **52**, R15 727 (1995).

<sup>3</sup>T. R. Chien, W. R. Datars, B. W. Veal, A. P. Paulikas, P. Kostic, C. Gu, and Y. Jiang, *Physica C* **229**, 273 (1994).

<sup>4</sup>J. A. Fendrich, W. K. Kwok, J. Giapintzakis, C. J. van der Beek, V. M. Vinokur, S. Fleshler, U. Welp, H. K. Viswanathan, and G. W. Crabtree, *Phys. Rev. Lett.* **74**, 1210 (1995).

<sup>5</sup>G. Blatter, M. V. Feigel'man, V. B. Geshkenbein, A. I. Larkin, and V. M. Vinokur, *Rev. Mod. Phys.* **66**, 1125 (1994).

<sup>6</sup>W. Jahn, S. N. Gordeev, C. Lessing, H. Küpfer, T. Wolf, M. Kläser, H. Wühl, G. Müller-Vogt, P. A. J. de Groot, and R. M. Langan, *Low Temp. Phys.* **105**, 1177 (1996).

<sup>7</sup>A. A. Zhukov, H. Küpfer, G. Perkins, L. F. Cohen, A. D. Caplin, S. A. Klestov, H. Claus, V. I. Voronkova, T. Wolf, and H. Wühl, *Phys. Rev. B* **51**, 12 704 (1995); H. Küpfer, T. Wolf, A. A. Zhukov, A. Will, C. Lessing, and R. Meier-Hirmer, in *Proceedings of the 8th International Workshop on Critical Currents in Superconductors*, Kitakyushu, Japan, 1996, edited by T. Matsushita and K. Yamafuji (World Scientific, Singapore, 1996), p. 349.

<sup>8</sup>A. Erb, J.-Y. Junoud, F. Marti, M. Däumling, E. Walker, and R. Flükiger, *J. Low Temp. Phys.* **105**, 1023 (1996).

<sup>9</sup>K. Deligiannis, P. A. J. de Groot, M. Oussena, S. Pinfold, R. Langan, R. Gagnon, and L. Taillefer, *Phys. Rev. Lett.* **79**, 2121 (1997).

<sup>10</sup>H. Safar, P. L. Gammel, D. A. Huse, D. J. Bishop, J. P. Rice, and D. M. Ginsberg, *Phys. Rev. Lett.* **69**, 824 (1992); W. K. Kwok, S. Fleshler, U. Welp, V. M. Vinokur, J. Downey, G. W. Crabtree, and M. M. Miller, *ibid.* **69**, 3370 (1992); M. Charalambous, J. Chaussy, P. Lejay, and V. M. Vinokur, *ibid.* **71**, 436 (1993).

<sup>11</sup>H. Safar, P. L. Gammel, D. A. Huse, D. J. Bishop, W. C. Lee, J. Giapintzakis, and D. M. Ginsberg, *Phys. Rev. Lett.* **70**, 3800 (1993).

<sup>12</sup>A. Junod, M. Roulin, B. Revaz, A. Mirmelstein, J.-Y. Junoud, E. Walker, and A. Erb, *Physica C* **282–287**, 1399 (1997); M. Roulin, A. Junod, A. Erb, and E. Walker, *Phys. Rev. Lett.* **80**, 1722 (1998).

<sup>13</sup>R. Gagnon, C. Lupien, and L. Taillefer, *Phys. Rev. B* **50**, 3458 (1994).

<sup>14</sup>J. R. LaGraff and D. A. Payne, *Physica C* **212**, 478 (1993); T. B. Lindemer, J. F. Hunley, J. E. Gates, A. L. Sutton, J. Brynestad, C. R. Hubbard, and P. K. Gallagher, *J. Am. Ceram. Soc.* **72**, 1775 (1989).

<sup>15</sup>R. M. Langan, S. N. Gordeev, M. Oussena, P. A. J. de Groot, A. G. M. Jansen, R. Gagnon, and L. Taillefer (unpublished).

<sup>16</sup>A. Schilling, R. A. Fisher, N. E. Phillips, U. Welp, D. Dasgupta, W. K. Kwok, and G. W. Crabtree, *Nature (London)* **382**, 791 (1996); M. Roulin, A. Junod, and E. Walker, *Science* **273**, 1210 (1996); U. Welp, J. A. Fendrich, W. K. Kwok, G. W. Crabtree, and B. W. Veal, *Phys. Rev. Lett.* **76**, 4809 (1996).

<sup>17</sup>G. Blatter, D. B. Geshkenbein, and A. I. Larkin, *Phys. Rev. Lett.* **68**, 875 (1992); Z. Hao and J. R. Clem, *Phys. Rev. B* **46**, 5853 (1992).

<sup>18</sup>S. Fleshler, W. K. Kwok, U. Welp, V. M. Vinokur, M. K. Smith, J. Downey, and G. W. Crabtree, *Phys. Rev. B* **47**, 14 448 (1993); J. N. Li, A. A. Menovsky, and J. J. Franse, *ibid.* **48**, 6612 (1993).

- <sup>19</sup>D. S. Fisher, M. P. A. Fisher, and D. A. Huse, *Phys. Rev. B* **43**, 130 (1991).
- <sup>20</sup>W. K. Kwok, S. Fleshler, U. Welp, V. M. Vinokur, J. Downey, G. W. Crabtree, and M. M. Miller, *Phys. Rev. Lett.* **69**, 3370 (1992).
- <sup>21</sup>J. Hofer, J. Karpinski, M. Willemin, G. I. Meijer, E. M. Kopnin, R. Molinski, H. Schwer, C. Rossel, and H. Keller, *Physica C* **297**, 103 (1998).
- <sup>22</sup>B. I. Ivlev and N. B. Kopnin, *Phys. Rev. B* **42**, 10 052 (1990); *Europhys. Lett.* **15**, 349 (1991).
- <sup>23</sup>D. R. Nelson, *Phys. Rev. Lett.* **60**, 1973 (1988); D. R. Nelson and H. S. Seung, *Phys. Rev. B* **39**, 9153 (1989).
- <sup>24</sup>Kwok *et al.* [W. K. Kwok, J. Fendrich, U. Welp, S. Fleshler, J. Downey, and G. W. Crabtree, *Phys. Rev. Lett.* **72**, 1088 (1994)] observed strong suppression of the resistivity due to intrinsic pinning of the vortex lines in detwinned  $\text{YBa}_2\text{Cu}_3\text{O}_{7-\delta}$  single crystals in the geometry  $H\parallel ab$ . We have not seen this effect in our samples.
- <sup>25</sup>B. Khaykovich, M. Konczykowski, E. Zeldov, R. A. Doyle, D. Majer, P. H. Kes, and T. W. Li, *Phys. Rev. B* **56**, R517 (1997).
- <sup>26</sup>D. R. Nelson and V. M. Vinokur, *Phys. Rev. B* **48**, 13 060 (1993).
- <sup>27</sup>T. Giamarchi and P. Le Doussal, *Phys. Rev. B* **55**, 6577 (1997); V. M. Vinokur, B. Khaykovich, E. Zeldov, M. Konczykowski, R. A. Doyle, and P. H. Kes, *Physica C* **295**, 209 (1998).